Journal of Materials Chemistry A

ROYAL SOCIETY OF CHEMISTRY

PAPER

View Article Online
View Journal

Cite this: DOI: 10.1039/d6ta02981g

Unraveling the lithium loss mechanisms during the high-temperature solid-state synthesis of ternary lithium-ion cathode materials

Siebe Coessens, *[a] Inge Bellemans, [a] Tijl Crivits, [b] Christophe Detavernier [c] and Kim Verbeken *[a]

Lithium losses during high-temperature synthesis of Nickel Manganese Cobalt (NMC) cathode materials are commonly attributed to lithium oxide (Li_2O) evaporation, based on early investigations of $Li_xNi_{1-x}O$ solid solutions. A critical review of this literature reveals, however, that the reported vapor pressures of Li_2O and Li_2O_2 are far too low to account for the experimentally observed mass losses under typical sintering conditions, and that Li_2O_2 itself is thermally unstable above 400 °C. This work re-examines the origins of lithium losses through thermodynamic equilibrium calculations and targeted calcination experiments. Calculations in the Li–O system confirm that gaseous lithium species remain negligible below 1500 °C, though even trace moisture significantly enhances lithium volatility *via* LiOH(g) formation. Nevertheless, predicted evaporative losses under realistic synthesis conditions remain below 0.1 mol%, far less than the 1–10 mol% typically reported. Complementary calcination experiments demonstrate that the dominant source of lithium depletion is solid-state reaction between the cathode precursor and the crucible material. Lithium readily reacts with common oxidic substrates such as Al_2O_3 and SiO_2, with losses scaling with contact area, whereas chemically inert substrates (MgO, Au) effectively suppress depletion. These results demonstrate that the widely accepted attribution of lithium loss to Li_2O evaporation is incorrect: substrate reactivity, not volatilization, is the dominant loss mechanism during NMC cathode synthesis.

Received 8th April 2026
Accepted 11th June 2026

DOI: 10.1039/d6ta02981g

rsc.li/materials-a

1 Introduction

Lithium-ion batteries (LIBs) have become the cornerstone of modern energy storage solutions, powering everything from portable consumer electronics to electric vehicles.[1–3] Among the various cathode materials, Nickel Manganese Cobalt (NMC) oxides have long stood out due to their high energy density, stability, and cost-efficiency. As the global demand for energy storage technologies continues to grow, so does the need for fundamental understanding on the synthesis mechanisms for cathode active materials, as this would allow facilitating more efficient production technologies.[2–4]

NMCs are prepared by a multi-step process in which one or more high-temperature steps play a key role. The transition-metal precursor ($Ni_xMn_yCo_{1-x-y}(OH)_2$) is usually obtained from a precipitation process and subsequently calcined with LiOH or Li_2CO_3 at temperatures between 600 °C and 1000 °C.[5,6] This sintering reaction is often referred to as the lithiation step, where Li diffuses into the transition-metal precursor to form a layered oxide with characteristic rhombohedral crystal structure (space group $R\bar{3}m$). Understanding on the underlying reaction mechanism of this calcination reaction has grown considerably over the last decade, thanks to increasing availability of advanced characterization techniques such as synchrotron-based *in situ* X-ray diffraction (XRD), simultaneous thermal analysis (STA) and secondary ion mass spectrometry (SIMS).[7–10] However, kinetic control of the high temperature reaction, as well as the ability to fine-tune the quality of the product remains notoriously difficult, due to the inherent complexity of the heterogeneous reaction mechanism that occurs between the lithium- and the transition-metal precursors at elevated temperatures.

One issue that has long been described in literature is the volatilization of lithium during the sintering step.[11–13] These lithium-losses are known to disrupt the formation of the layered structure of the NMC material, as large lithium deficiencies promote the formation of spinel and rock salt phases, which are detrimental to the mobility of lithium-ions within the material, effectively reducing the resulting capacity.[14,15] The structural instability caused by lithium losses can also result in

[a]Department of Materials, Textiles and Chemical Engineering, Ghent University, Technologiepark 46, 9052 Zwijnaarde (Gent), Belgium. E-mail: Inge.Bellemans@ugent.be; Kim.Verbeken@ugent.be
[b]Umicore Rechargeable Battery Materials Belgium, Watertorenstraat 33, 2250 Olen, Belgium
[c]Department of Solid State Sciences, Ghent University, Krijgslaan 281 S1, 9000 Gent, Belgium

mechanical degradation, such as cracking and particle pulverization, further reducing the cycling life of the battery. An obvious solution to mitigate lithium volatilization is the addition of excess lithium in the precursor blend to compensate for high temperature losses. While this strategy is commonly applied in literature, recommendations for the optimal Li-excess vary strongly among different authors.[16–18] Careful control of the amount of excess lithium is crucial to avoid introducing impurities and maintaining the overall quality of the NMC material. Kim *et al.* demonstrated that residual lithium oxide on the surface of primary NMC particles reacts with moisture, and CO_2 in the environment to form an insulating layer of LiOH and Li_2CO_3, which impedes the diffusion of lithium ions, thereby deteriorating electrochemical properties.[19] These observations exemplify the importance of understanding and quantifying the mechanisms by which lithium losses occur during sintering.

Lithium losses from layered lithium transition metal oxides ($LiTMO_2$) species during the synthesis of NMC materials have been a topic of considerable research and debate throughout the last few decades. Traditional studies, such as those by Sata[11] and Antolini,[12] have suggested that lithium losses can be primarily attributed to the evaporation of Li_2O at elevated temperatures. These studies have provided valuable insights into the kinetics of lithium losses from $Li_xNi_{1-x}O$. However, a critical examination of the literature from different research fields contradicts this suggestion by proving that the vapor pressure at temperatures below 1000 °C is negligibly low, suggesting that lithium losses through gas-phase evaporation should be minimal under the conditions relevant for NMC synthesis.[20–22]

This paper re-examines the origins of lithium losses during the synthesis of NMC cathode materials and demonstrates that Li_2O evaporation is thermodynamically negligible under industrially relevant calcination conditions. Instead, we show that the dominant lithium loss mechanism is solid-state reaction between the cathode precursor and the substrate material. For instance, lithium oxide can react with alumina (Al_2O_3) to form lithium aluminate ($LiAlO_2$), leading to lithium losses that cannot be accounted for by evaporation alone. By critically analyzing the existing literature, thermodynamic equilibrium calculations, and experimental data, this paper seeks to provide a comprehensive understanding of the mechanisms driving lithium losses during NMC synthesis, offering insights into optimizing synthesis conditions to minimize these losses and enhance the efficient production and hence ultimately the performance of NMC cathode materials.

2 Mechanism of lithium evaporation

There is no shortage of studies on the high temperature behavior of Li_2O in various energy storage materials. Most notable in the context of ternary lithium ion cathode materials, is the work of Sata[11] and Antolini,[12,23–26] who performed extensive investigations into the mechanisms of lithium oxide evaporation from solid solutions. Their findings are still widely cited in recent studies to explain the need for excess lithium during NMC synthesis.[8,27–29]

Sata was the first to systematically investigate the mechanism responsible for lithium losses from $Li_xNi_{1-x}O$ solid-solutions at high temperatures. In this study, sintered $Li_xNi_{1-x}O$ disks of varying composition ($x \leq 0.4$) were subjected to vaporization experiments, in which samples were placed in a mullite reaction tube and kept at constant temperatures in the range of 400 °C–700 °C under a steady flow of air. The weight loss that occurred during each annealing cycle was assessed by measuring total sample mass before and after the anneal with a microbalance, and the final lithium content (x-value) of the solid-solution was obtained through Rietveld refinement of XRD patterns after final annealing. Additionally, XRD patterns were recorded through the thickness of each specimen to analyze the composition gradient. The experiments confirmed that the lithium content of the solid solutions decreased with increasing temperature and annealing times. Based on these observations, Sata proposed the following equations to describe the observed weight loss:

$$Li_xNi_{1-x}O \leftrightarrow a[Li_yNi_{1-y}O] + bLi_2O + cO_2 \quad (1)$$

$$Li_2O(s) + O_2 \leftrightarrow Li_2O_2(g) \quad (2)$$

where $a = \frac{(1-x)}{(1-y)}$, $b = \frac{(x-y)}{2(1-y)}$, $c = \frac{(x-y)}{4(1-y)}$ and with $x > y$. The mechanism is thus based on the hypothesis that weight loss corresponds to the sum of the Li_2O and O_2, due to their subsequent reaction to form gaseous Li_2O_2. This assumption is, in turn, based on the fact that the vapor pressure of Li_2O_2 was reported to be much higher than that of Li_2O, and strengthened by the similarity of the calculated activation energy from the Arrhenius plot of the observed evaporation rate (344 kJ mol^{-1}), and the heat of sublimation of $Li_2O(s)$ to $Li_2O_2(g)$ (356 kJ mol^{-1}) cited from literature. From the measured mass loss, an apparent three stage evaporation mechanism was observed: in the first stage limited weight loss is observed due to formation of Li_2O, which is accompanied by O_2 release according to eqn (1). It is alleged this process leads to formation of a Li_2O gradient, with higher concentrations building at the sample surface. In the second stage, it is supposed that the formation and diffusion of $Li_2O_2(g)$ becomes the rate-determining step and is responsible for the bulk of the observed mass loss. The vaporization stopped in the third stage, and the author concluded that at this point the dissolution equilibrium of eqn (1) has been reached.

Furthermore, Sata observed the value of x in $Li_xNi_{1-x}O$ linearly decreases from the surface to the interior of the specimen and hypothesized that the formation of Li_2O_2 from Li_2O may be the rate-determining step in the lithium loss process, rather than the diffusion of Li-ions to the surface. While the observations from this work are valuable in quantifying lithium losses from $Li_xNi_{1-x}O$ solid solutions and the proposed mechanism seems reasonable, it should be noted that the referenced vapor pressures of lithium oxides are very low. At 1000 K and a p_{O_2} of 0.2 bar, the mentioned vapor pressures are $Li_2O_2(g)$ =

2.7×10^{-6} Pa, LiO(g) = 6.2×10^{-8} Pa and Li_2O(g) = 3.1×10^{-8} Pa. Taking the vapor pressure of Li_2O_2 listed in the study, it is possible to calculate the theoretical gas volume that would be required to account for the observed mass loss (order of magnitude 10^{-4} to 10^{-3} g) *via* an evaporation mechanism. Assuming ideal gasses and a system at thermodynamic equilibrium at all times (infinitely fast kinetics), one can find that it would take a total gas volume of 2.0×10^4 m^3 to evaporate a sufficient amount of Li_2O_2 at 1000 K. At a flow rate 200 cm^3 min^{-1} (listed in the work under discussion) this would take approximately 190 years. The details of this calculation can be found in section S1 of the SI.

More recent investigations on the stability and formation of Li_2O_2 raise further questions about the proposed mechanism. Rodriguez *et al.*[30] investigated high-temperature oxidation behavior of Li powder in O_2/Ar atmosphere (10% O_2). Analysis of mass gain during TGA experiments revealed that while Li initially oxidizes to a mixture of Li_2O and Li_2O_2 at temperatures < 400 °C, only Li_2O forms at higher temperatures. This is consistent with multiple reports on the thermal stability of Li_2O_2, which verified independently that the decomposition of Li_2O_2 to Li_2O occurs between 280 °C and 400 °C.[31–33] Furthermore, TGA experiments indicated that Li_2O retains stable mass up to 1200 °C, with a minor weight loss at 450 °C attributed to impurity decomposition. While the loss of lithium during high temperature sintering observed by Sata cannot be denied, this raises questions about the accuracy of the proposed mechanism. This is a relevant concern as without proper description of the mechanism, it is difficult to design mitigation strategies for lithium losses.

Antolini investigated independently the evaporation of lithium oxide from $Li_xNi_{1-x}O$ solid solutions and later expanded upon the work of Sata.[12,26] In contrast to Sata's work, where lithium losses from pre-prepared solid solutions were observed, Antolini studied directly the lithium losses that occurred during the annealing of NiO/Li_2CO_3 mixtures at various temperatures and mixture compositions. A similar methodology was used as before, where lithium losses are evaluated through Rietveld refinement of XRD pattern, recorded after TGA experiments for various times and temperatures. Their first study compared lithium losses in mixtures with nominal Li content 0.20 and 0.30 and found that the mechanism is diffusion-controlled as it is governed by a parabolic law:

$$x_{ev}^2 = K(t - t_0)$$

where x_{ev} is the cationic fraction of Li^+ that evaporated, K is the rate constant, and $(t - t_0)$ is the annealing time. It was found that K decreases with the nominal lithium content and that a temperature exists dependent critical lithium content x_c, at which lithium losses are no longer observed: 0.28 at 745 °C and 0.08 at 830 °C. In later work, Antolini went on to measure the kinetics of lithium loss at higher temperatures and found that at 900 °C lithium losses from solid solutions could be fit to a simple kinetic equation:

$$x_{ev} = kt^n$$

where x_{ev} is again the observed lithium loss, k is the rate constant, t is time, and n is related to the reaction mechanism. Diffusion controlled evaporation is described by $n = 0.5$ to 0.8. Log–log plots of lithium loss *vs.* time were fit by two lines with slopes $n = 0.75$ and $n = 0.48$: A two-step mechanism where both steps are diffusion controlled. The results were interpreted as rapid lithium diffusion along grain boundaries ($n = 0.75$), followed by more sluggish lithium diffusion from the bulk towards lithium-poor grain boundaries ($n = 0.48$). While the observations from XRD with respect to lithium losses in the solid-solutions are undeniable, it remains unclear if the proposed mechanism for evaporation is feasible given the low vapor pressures of Li–O compounds under typical sintering conditions.

Iida[20] studied evaporation of Li_2O from a $Li_xNi_{1-x}O$ solution with $x = 0.15$, and observed that evaporation of Li_2O from this solution was negligibly small at 1000 °C and increased with increasing temperature. This observation is in agreement with more fundamental investigations of the thermodynamics that govern the Li–O system. Van Arkel[34] investigated the evaporation of pure Li_2O by heating powder samples in a platinum crucible on a precision balance and noted that no mass loss could be observed from *in vacuo* experiments at 1000 °C. The author additionally noted that during experiments on molten Li_2O at 1570 °C there was no indication that the vapor pressure was significant. Watari *et al.*[35] studied the volatility of Li_2O in the context of using it as a sintering aid during the synthesis of AlN ceramics. In mixtures containing 10 wt% Li_2O they noticed no volatilization below 1300 °C, while Li content decreased to the ppm level after heating to 1600 °C. Hoshino *et al.*[36] observed limited lithium losses during the synthesis of lithium titanate ($Li_{2+x}TiO_{3+y}$) and LTZO ($Li_{2+x}(Ti,Zr)O_{3+x}$) pebbles at 1100 °C under air. If one thing should be clear from this literature discussion, it is that there exist a significant number of contradicting reports about both the severity and the cause of lithium loss from solid solutions at high temperatures. While the systemic quantifications performed by Sata and Antolini are sound, the underlying mechanism of evaporation is debatable when considering observations from related research fields. Since the lithium losses are in fact observed, some other mechanisms must play a role.

McCalla *et al.*[13] conducted a comprehensive study on the mechanism of lithium loss during and after the synthesis of combinatorial $Li_xNi_{2-x}O_2$ samples (with x close to unity), which were co-precipitated from stoichiometric Li- and Ni-nitrate solutions and subsequently calcined at high temperature. The tested variables included: the heating atmosphere (argon, air and O_2), heating temperature, the chemical used for precipitation (ammonium bicarbonate or ammonium hydroxide), and the substrate material (Al_2O_3, MgO and $LiAlO_2$). Lithium losses were determined from Rietveld refinement of the XRD patterns. The authors identified two distinct mechanisms that could explain the observed decrease in lithium content. The first was the thermal decomposition of lithium nickel oxide at high temperature according to eqn (1), which was revealed with TGA: All $Li_xNi_{2-x}O_2$ samples showed continuous mass loss during annealing at 600 °C, 700 °C and 800 °C. The heating

atmosphere was found to significantly impact the decomposition rate (and hence rate of lithium loss from the solid solution), with slower reaction kinetics in O_2 as compared to air and argon. Loss of lithium was again attributed to Li_2O_2 vapor formation but not directly observed. The second mechanism of lithium loss observed was the decomposition of Li_2CO_3 that was shown to form during synthesis (even with the limited carbon present in the system) and subsequently failed to react with nickel oxide below its decomposition temperature. Again, this mechanism led to much higher losses in air compared to pure O_2. Interestingly, further experiments showed that the oxygen partial pressure itself played only a small role, as high lithium contents could be obtained using a synthetic gas mixture of 5.5% O_2 and 94.5% N_2. The authors suggested that the presence of CO_2 and potentially H_2O in air inhibits the formation of lithium nickel oxide, rather than low O_2 content. While not detailed as a separate mechanism of lithium loss by the authors, there was a clear effect of the substrate material on lithium loss for samples calcined in air. For all samples the observed lithium loss was extreme: 47% on alumina at 700 °C, reduced to approximately 32% by using either MgO or alumina pre-treated with lithium hydroxide ($LiAlO_2$). The authors ascribe the poor performance of the alumina substrate to the reaction of unreacted lithium in the samples to form $LiAlO_2$. This observation has important implications on the studies discussed so far, as substrate materials vary between the different literature data including alumina, mullite, silica and platinum.

Interestingly, McCalla *et al.*[13] observed that for samples prepared in pure O_2 the substrate did not seem to have a pronounced effect. This observation has important implications on the studies previously discussed, as substrate materials used to study Li–O volatilization vary between authors and are not always mentioned (*e.g.* Iida – Pt; Van Arkel – Pt; Antolini – quartz/alumina; Sata – mullite/alumina). Similarly, Lan *et al.*[37] investigated the contamination of alumina crucibles during the sintering process of $Li_7La_3Zr_2O_{12}$ (LLZO) solid electrolytes, focusing on the role of excess Li_2CO_3. The study highlights that the presence of excess Li_2CO_3 in the LLZO powder leads to the formation of Al-containing impurities, specifically $LiAlO_2$, due to the reaction between pyrolytic Li_2O from Li_2CO_3 and alumina at high temperatures. This reaction results in a liquid Li–Al–O eutectic, which promotes the dissolution of the aluminum oxide crucible and affects the compactness and distribution of Al in the pellets, and resulting in undesired phase transformations. The findings show that using excess Li_2CO_3 leads to increased substrate reactivity and the formation of $LiAlO_2$ impurities, which gather at grain boundaries and affect the morphology and electronic conductivities of the pellets. The study concludes that while adding extra Li_2CO_3 can compensate for lithium loss during sintering, the amount must be carefully regulated to balance pellet density and phase stability.

Recently, Wu *et al.*[29] reported that Li_2O can sublimate at 850–900 °C under 1 atm O_2 and demonstrated that Li_2O vapor can lithiate transition-metal oxide (TMO) precursors without direct physical contact in a sealed crucible experiment. The authors invoke the Kelvin equation to argue that porous Li_2O particles exhibit enhanced vapor pressures, and that the chemical reaction with TMO continuously shifts the solid–vapor equilibrium. In the absence of a TMO sink, the authors report a mass loss of 2.7 wt% from pure Li_2O at 870 °C over 10 h, which they attribute to self-sintering that limits further sublimation. However, as will be shown in section 4.1, this observed mass loss exceeds thermodynamic predictions for pure Li_2O sublimation by several orders of magnitude, suggesting that additional mechanisms, such as moisture-induced LiOH(g) volatilization, likely contribute to the reported loss. Notably, the *in situ* XRD characterization of a blended Li_2O/TMO system presented by Wu *et al.* (Fig. 3a in 29) reveals that LiOH is present at low temperatures (attributed by the authors to brief air exposure) and that Li_2O is fully consumed through solid-state reaction by 500 °C, confirming that when lithium precursor and TMO are in direct contact, lithiation proceeds through conventional solid-state diffusion well below the temperatures at which gas-phase transport becomes relevant.

In conclusion, three notable lithium loss mechanisms are mentioned when looking at the available literature on high temperature calcination reactions involving lithium precursors: (1) Evaporation of expected lithium species at high temperature, in particular: Li_2O_2, Li_2O and LiO. (2) Volatilization of unexpected lithium species due to the presence CO_2 and H_2O in the calcination atmosphere at high temperatures. (3) Loss of lithium due to solid–solid/solid–liquid interactions between lithium compounds and the substrate material used for calcination. The purpose of the current study is to thoroughly assess which of these mechanisms plays the dominant role during high temperature NMC synthesis, by analyzing the available thermodynamic data on the system combined with experimental observations from both TGA and ICP analysis of NMC samples prepared under varying conditions.

3 Materials and methods

3.1 Thermodynamic calculations

Thermodynamic calculations were performed using FactSage software (version 8.3), which integrates extensive empirical databases and Gibbs free energy minimization algorithms to determine the thermodynamic equilibrium conditions of a given system.[38,39] The Equilib module was employed to simulate equilibrium compositions and phase distributions of relevant Li–O–H systems, under varying temperatures, O_2 and H_2O partial pressures, representative of both laboratory and industrial cathode synthesis environments. Thermodynamic data was sourced from the FactPS en FToxid databases, which provide reliable information for the pure substances and oxide phases. These calculations enable the prediction of volatile species formation and their dependence on process parameters, offering insights into material losses and atmosphere control during synthesis. Inputs and considered phases for the equilibrium calculations are mentioned where necessary and detailed in Tables S1–S4 of the SI. Systems were studied in the temperature range of 0 °C to 2000 °C under atmospheric pressure.

3.2 Thermogravimetric analysis

Thermogravimetric analysis (TGA) was performed on a TA Instruments SDT 650 to verify the absence of measurable mass loss during isothermal calcination. A stoichiometric NMC($9\frac{11}{22}$) blend (LiOH + $TM(OH)_2$), was loaded into an MgO crucible (85 μL) under O_2 flow (100 mL min^{-1}). The sample was heated at 50 °C min^{-1} to 900 °C and held isothermally for 60 minutes. Mass was normalized to the value recorded at 100 °C after a 30 minute baseline hold to exclude physisorbed moisture.

3.3 Calcination experiments

Calcination experiments are performed in a gas-tight atmosphere furnace (GAF) in order to quantify lithium losses during high temperature synthesis. In our previous work, we illustrated that lithium compounds react with most ceramic substrate materials, leading to significant lithium loss.[40] The calcination experiments in this work serve to further quantify how these interactions contribute to the total lithium loss during calcination, and how it compares to lithium loss through other mechanisms. Five distinct sets of calcination experiments (C1 – C5) were performed, as detailed below (and summarized in Table 1). In each set, NMC blend samples were subjected to an identical calcination cycle in a gas tight atmosphere furnace (GAF) at 900 °C for 10 hours in a 10 l min^{-1} O_2 flow (>99.5%). For the preparation of the NMC blends, LiOH (>99 wt%) and an oxide precursor with a nominal composition of $Ni_{0.8}Mn_{0.1}Co_{0.1}O$, were mixed through ball milling to obtain a fine NMC811 blend. By using a pre-calcined oxide as precursor, an additional moisture source is eliminated, meaning that the lithium losses reported in this work are if anything underestimated relative to what would occur with a hydroxide precursor under otherwise identical conditions. The LiOH and (Ni, Mn, Co)O powders were weighed on a precision balance and premixed with a target Li : M molar ratio of 1.04. The mixture was ball milled using zirconia balls (φ = 5 mm) for 3 hours to obtain a homogeneous blend.

Calcination experiment **C1** serves as a qualitative test and proof of concept to verify that the contact surface area between substrate and powder blend affects high temperature lithium loss. Two calcination experiments are compared. The first experiment serves as the reference in which 100 g NMC blend is calcined in a standard alumina crucible with dimensions 10 × 10 × 7 cm. In the second experiment, a sample of the same mass is calcined under identical conditions. However, the contact surface area between the NMC precursor blend and the alumina crucible is artificially increased by submerging a second, fragmented alumina crucible within the powder blend, roughly doubling the contact surface area.

Calcination experiment **C2** was designed based on the results of **C1** and serves to more accurately quantify the surface area effect. Increasing blend masses were placed in fresh crucibles in order to vary the contact surface area to mass ratio (A m^{-1}) between the substrate and the powder blend. Small cylindrical crucibles are used for these experiments so that the total contact surface area can be accurately evaluated by measuring the powder height in each crucible. This test was performed for three different crucible materials: alumina (Al_2O_3), silica quartz (SiO_2 Q) and a high porosity silica fiber (SiO_2 F) crucible. These materials were chosen because they are commonly used for small scale high temperature investigations, and their interaction with NMC blend was clearly demonstrated in our earlier work. The specifications of the crucible materials are listed in Tables S5–S7 of the SI. For each substrate material, three A m^{-1} ratios were tested within the range of 50–500 mm^2 g^{-1}.

Calcination experiment **C3** is a standard calcination experiment in which 100 g of blend was calcined in a wide alumina crucible (10 × 10 × 7 cm), resulting in an A m^{-1} ratio of approximately 100 mm^2 g^{-1}. Layers of the calcined NMC are sampled separately from top to bottom to identify and analyze the gradient of lithium throughout the sample. Layers of approximately 2 mm are carefully scraped from the sintered powder bed with a scalpel and analyzed individually.

Calcination experiment **C4** aims to illustrate the effect of H_2O vapor pressure on high temperature lithium losses. As the GAF setup does not allow direct injection of steam, a recipient containing 2 L of water was placed inside the furnace alongside the NMC blend in different crucibles, to saturate the furnace atmosphere with H_2O. The chemical composition and

Table 1 Summary of calcination experiments performed in this work. All experiments use NMC811 blend (LiOH + $Ni_{0.8}Mn_{0.1}Co_{0.1}O$, target Li : M = 1.04) calcined in a gas-tight atmosphere furnace

Exp.	Objective	Substrate(s)	Key variable	Blend mass	A/m ratio	Conditions
C1	Qualitative proof that contact surface area affects Li loss	Al_2O_3	Contact surface area	100 g	≈100 mm^2 g^{-1}	900 °C, 10 h, 10 l min^{-1} O_2
C2	Quantitative relationship between A/m ratio and Li loss	Al_2O_3, SiO_2 (quartz), SiO_2 (fiber)	A/m ratio (50–500 mm^2 g^{-1})	Variable	50–500 mm^2 g^{-1}	900 °C, 10 h, 10 l min^{-1} O_2
C3	Depth-resolved Li : M gradient through sintered powder bed	Al_2O_3	ICP sampling depth (0–1.2 cm)	100 g	≈100 mm^2 g^{-1}	900 °C, 10 h, 10 l min^{-1} O_2
C4	Effect of H_2O vapor pressure on Li loss and electrochemical performance	Al_2O_3, SiO_2 (Q), SiO_2 (F), MgO, Au	Atmosphere (dry O_2 *vs.* H_2O-saturated O_2)	10 g	≈250 mm^2 g^{-1}	900 °C, 10 h, 10 l min^{-1} O_2
C5	Effect of repeated crucible use on Li loss (substrate saturation)	Al_2O_3, MgO	Number of prior uses (fresh, ×1, ×2)	10 g	≈250 mm^2 g^{-1}	900 °C, 10 h, 10 l min^{-1} O_2

electrochemical performance of the samples from this experiment were tested in coin cells and compared to references samples synthesized under identical, but dry conditions. The selected crucibles stem from our previous investigation on substrate-induced lithium losses and include the oxide refractories: α-Al_2O_3 corundum, SiO_2 quartz and SiO_2 fiber, MgO periclase and high purity Au. These substrates are selected because the mixed oxides mullite ($3Al_2O_3 \cdot 2SiO_2$) and cordierite ($Mg_2Al_4Si_5O_{18}$) are commonly used as saggar materials for industrial high-temperature calcination processes, while their pure oxide forms are common substrate materials for laboratory-scale experiments for a variety of applications. Au serves as a reference due to its known chemical stability and resistance against high temperature oxidation.

Calcination experiment **C5** investigates the effect of repeated crucible use on lithium losses during calcination. NMC blend samples of 10 g were calcined in small cylindrical crucibles (8 mL) of two different materials: α-Al_2O_3 and MgO. For each crucible material, three sequential calcination cycles were performed in the same crucible without intermediate cleaning, using fresh NMC blend for each cycle. After each cycle, the calcined product was removed, and the crucible was reloaded with a new batch of blend for the subsequent calcination. In this way, any lithium-containing reaction products (*e.g.* $LiAlO_2$) formed at the crucible interface during earlier cycles remain in place, progressively passivating the reactive surface. All other calcination conditions were identical to those of experiments C1–C4. The experiment was repeated three times for MgO and twice for Al_2O_3. For the Al_2O_3 experiments, ICP-OES was additionally used to quantify the Al content in the calcined NMC product as an independent measure of crucible–powder interaction.

3.4 Inductively coupled plasma optical emission spectroscopy (ICP-OES)

For all described experiments the lithium to transition metal ratios (Li : M) were determined using Inductively Coupled Plasma Optical Emission Spectroscopy (ICP-OES) before and after calcination to determine the amount of lithium lost during each calcination cycle. The measurements are performed on an Agilent 5110 ICP-OES spectrometer. Solutions are prepared by dissolving ground powder samples of 0.2 g in 5 mL HCl and 3 mL HNO_3, adding 2 mL of citric acid, 0.2 mL Sc (1 g L^{-1} internal standard), and diluting to 20 mL. The weight fractions of Li, Ni, Mn and Co are measured from which molar Li : M ratios could be calculated. Li-losses that occurred during calcination were quantified by comparing the molar Li : M ratio before and after the calcination cycle.

3.5 Electrochemical testing

To prepare positive electrodes from the samples of calcination experiment C4, synthesized cathode materials were combined with conductive carbon particles (Super P, Timcal) and a binder material (Kureha) in a mass ratio of 90 : 5 : 5. This mixture was homogenized using *N*-methyl-2-pyrrolidone (NMP, Mitsubishi) as the solvent and applied to one side of an aluminum current collector. The slurry coated foil is dried in an oven at 120 °C for 12 hours and pressed using a calendaring tool. Finally, the foils are dried again in a vacuum oven to completely remove the remaining solvent in the electrode film. Coin cells (type CR2032) were assembled in an argon-filled glovebox. A separator (Celgard) was placed between the positive electrode and a piece of lithium metal serving as the negative electrode. An electrolyte solution of 1M $LiPF_6$ in ethylene carbonate (EC) and dimethyl carbonate (DMC) in a volume ratio of 1 : 2 is dropped between the separator and the electrodes. The cells were cycled at 25 °C, using a computer-controlled galvanostatic cycling station. The testing procedure uses a 1C current definition of 160 mA g^{-1}. The charge and discharge conditions are detailed in Table S8 (SI).

4 Results and discussion

4.1 Theoretical volatility of lithium in a dry Li–O system

As discussed in section 1, observed lithium losses during cathode synthesis are usually attributed to the volatilization of Li_2O, the product of Li_2CO_3 or LiOH decomposition, into gaseous compounds such as LiO, Li_2O, and Li_2O_2. Accordingly, the starting point for a thermodynamic investigation of predicted lithium losses was the state-of-the-art thermodynamic data available in the FToxid database for these compounds. While the mapping of the thermodynamic properties of layered $LiMO_2$ materials is ongoing in the literature,[41,42] virtually none of this data is currently publicly available in thermodynamic software packages like FactSage. For this reason, no transition metal oxides (NiO, Mn_2O_3, CoO) were considered in the current calculations. This simplification is not expected to significantly impact the interpretation of lithium volatility, as the addition of transition metal oxides would primarily lower the activity of lithium within a solid or liquid solution. According to Raoult's law for ideal solutions, this would in turn lower the theoretical vapor pressure of lithium species in proportion to their mole fraction. It should be noted that real systems may deviate from ideality, especially at high temperatures and in complex oxide matrices, so that the presence of transition metal oxides could influence phase equilibria and reaction pathways in unexpected ways. Despite these limitations, the current approach provides a reasonable first-order approximation for assessing lithium volatility during cathode synthesis.

The calculated thermodynamic stability of Li_2O under an atmospheric pressure of O_2 is shown in Fig. 1. The system considers 0.5 mol of Li_2O in contact with 5 mol of O_2, which is representative of typical ratios used in mass production rotary or tunnel kilns (~1 Nm^3 (normal cubic meter, *i.e.* gas volume at 0 °C and 1 atm) of O_2 per kg NMC). Three distinct regions are readily observed: At low temperatures, lithium is most stable as solid lithium peroxide (Li_2O_2), which remains stable up to approximately 340 °C. Above this temperature, Li_2O_2 decomposes, and solid lithium oxide (Li_2O) becomes the stable phase. As the temperature increases further, Li_2O remains solid until it reaches its melting point. This transition occurs at approximately 1440 °C. Only at temperature above 1500 °C, various lithium compounds do have a notable presence within the gas

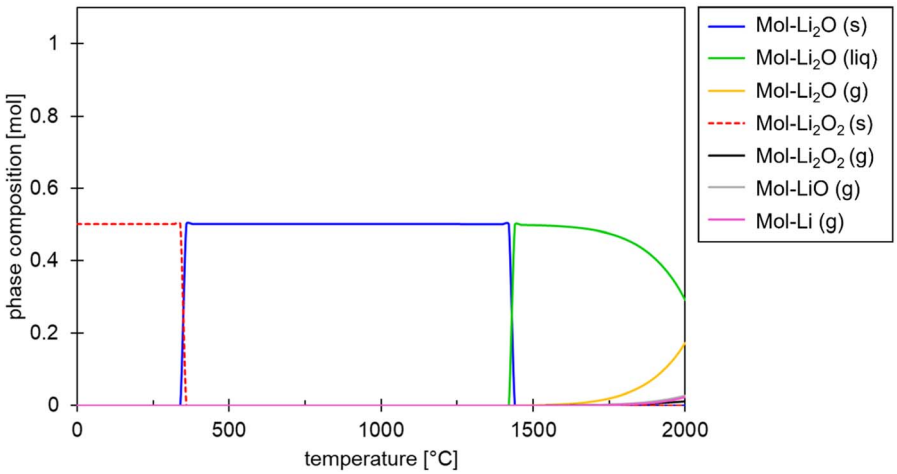

Fig. 1 Evolution of the equilibrium phase composition of 0.5 mol Li_2O under an O_2 atmosphere as function of temperature.

phase. While Li_2O(g) is the dominant species in the gas phase, Li_2O_2(g), LiO(g), and atomic Li(g), also gain a considerable presence at the highest temperatures shown.

Fig. 2a shows the calculated cumulative lithium loss to the gas phase (*i.e.* the stoichiometric sum of all predicted gaseous Li-compounds divided by total moles of lithium in the initial system). Fig. 2b shows the individual vapor pressures of each predicted gaseous compound in the equilibrium gas phase, in the temperature range relevant for NMC synthesis. The data labels marked on the graph show the vapor pressures of Li_2O_2 and Li_2O at 600 °C, 800 °C and 1000 °C. This data confirms that in the presence of O_2, the oxidation reaction Li_2O (s) + 1/2 O_2 ⇔ Li_2O_2 (g) is favored over the direct evaporation of lithium oxide by 1 – 3 orders of magnitude, so that volatilization of lithium is greatly enhanced in the presence of oxygen. However, the key observation from this equilibrium calculation is that the vapor pressures of all lithium-containing gaseous compounds—such as Li_2O(g), Li_2O_2(g), and LiO(g) (lithium monoxide, a diatomic radical species documented in the JANAF thermochemical tables[43])—remain remarkably low, with total lithium losses at equilibrium accounting for just 2.82 × 10^{-5} mol% at 1000 °C. This implies that, under an oxygen atmosphere at atmospheric pressure, and in the assumption that LiOH decomposes to Li_2O before reaching the temperature at which calcination takes place, lithium volatility is predicted to be negligible throughout the entire temperature range typically used for NMC cathode synthesis. Li_2O evaporation is therefore negligible throughout the entire temperature range used for NMC synthesis, with lithium remaining locked in the solid phase. Even at 1000 °C, total gaseous lithium accounts for only 2.82 × 10^{-5} mol%, five orders of magnitude below the 1–10 mol% losses routinely reported in the literature. This discrepancy rules out Li_2O volatilization as the dominant source of experimentally observed lithium depletion and points unambiguously to alternative loss mechanisms.

It should be noted that in practice, the LiOH precursor does not simply decompose to Li_2O and H_2O during heating; rather, it reacts directly with the transition-metal oxide/hydroxide precursor well below 700 °C, so that by the time the final calcination temperatures are reached, virtually all lithium has

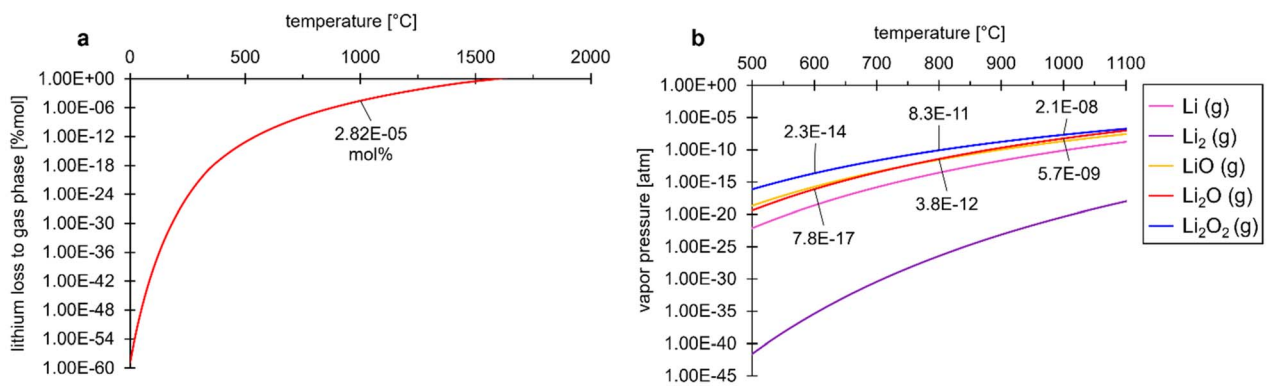

Fig. 2 Total lithium losses to the O_2–gas phase in a dry Li–O system (a). Vapor pressures of individual gaseous compounds that constitute the total lithium loss to the gas phase in the temperature interval relevant for NMC synthesis (b).

been incorporated into the layered structure.[8,44] Consequently, the Li_2O that may be thermodynamically available at high temperatures originates predominantly from thermal decomposition of the layered oxide itself according to the following reaction pathway:

$$LiTMO_2 \rightarrow (\delta/2)\ Li_2O + Li_{1-\delta}TMO_{2-\delta} + (\delta/4)\ O_2\uparrow \quad (3)$$

where δ denotes the extent of decomposition. This pathway becomes increasingly relevant at elevated temperatures and reduced oxygen partial pressures. The equilibrium calculations presented here assess the intrinsic volatility of Li_2O regardless of its origin. Since the predicted vapor pressures depend only on temperature and atmosphere composition, not on the reaction pathway by which Li_2O is formed, the conclusions remain valid irrespective of whether the Li_2O originates from precursor decomposition or from high-temperature NMC degradation. Moreover, in a decomposition scenario where Li_2O forms as a minority product within a predominantly layered oxide matrix, its thermodynamic activity is substantially lower than unity. According to Raoult's law, this further reduces the effective vapor pressure of lithium-containing gaseous species relative to the pure Li_2O system calculated here, making the present predictions a conservative upper bound for lithium volatility during NMC synthesis.

The thermodynamic predictions presented here provide important context for the recent work of Wu *et al.*,[29] who reported a 2.7 wt% mass loss from pure porous Li_2O heated at 870 °C for 10 h in O_2. This observed loss exceeds the equilibrium prediction by approximately five orders of magnitude (*cf.* Fig. 2a: 2.82×10^{-5} mol% at 1000 °C), indicating that the measured mass loss should not be attributed solely to Li_2O sublimation. The presence of LiOH detected in the authors' *in situ* XRD data (attributed to air exposure of the hygroscopic Li_2O prior to the experiment) suggests that moisture-induced LiOH(g) formation (discussed below in section 4.2) likely contributes significantly to the observed mass loss. While the Kelvin effect invoked by the authors can enhance the vapor pressure of nanoparticles, the bulk particle size reported (D50 = 32.9 μm) limits the magnitude of this enhancement to well below what would be required to account for the discrepancy. These considerations reinforce that the vapor pressure of Li_2O remains thermodynamically negligible under standard cathode synthesis conditions, and that lithium losses observed experimentally should be carefully deconvoluted from contributions by moisture-induced volatilization.

4.2 Theoretical volatility of lithium in a wet Li–O–H system

As discussed above, the LiOH precursor reacts with the transition-metal precursor well below the final calcination temperature, so that under ideal conditions all H_2O released during this decomposition is evacuated by the gas flow before reaching the high-temperature regime. The calculations in section 4.1 reflect this scenario by considering only Li_2O as the lithium-containing phase. However, in practice, complete removal of moisture cannot be guaranteed: diffusion limitations within the powder bed, incomplete gas exchange, and residual moisture in the gas supply may all result in trace amounts of H_2O persisting in the system at elevated temperatures. The next set of calculations shows how lithium volatility is impacted when H_2O remains present, by considering the equilibrium of the Li–O–H system. Fig. 3 shows the phase evolution of a closed system containing initially 1 mol LiOH in contact with 5 mol O_2 at atmospheric pressure. The data confirms that thermodynamically speaking, LiOH indeed decomposes in the relatively low temperature range between 300 °C and 640 °C. This range corresponds well with reports from literature.[45,46] However, from the further phase evolution, it becomes evident that in a closed system solid Li_2O readily recombines with H_2O at higher temperatures (>900 °C) to form an considerable amount of gaseous LiOH. Fig. 4a shows the cumulative lithium losses in this system and how it compares again the "dry" Li_2O system. The calculations show that in the presence of residual H_2O from the LiOH decomposition reaction, lithium losses to the gas phase increase by a factor 10^5 to 10^6 with respect to the dry system. Fig. 4b breaks down the individual vapor pressures in the Li–O–H system. The data reveals that the pressure of all components are essentially negligible when compared to the vapor pressure of LiOH(g) and $(LiOH)_2$(g) (the gas-phase dimer of lithium hydroxide, a well-documented association product of alkali hydroxide vapors[47]). For comparison, even at just 500 °C the vapor pressure of LiOH (2.7×10^{-9} atm, or 2.7 ppb) exceeds the vapor pressure of both Li_2O_2 and Li_2O at 900 °C (1.6×10^{-9} atm 2.0×10^{-10} atm, respectively). It is clear that lithium is much more volatile in its hydroxide state, than in its oxide state.

4.3 Influence of H_2O partial pressure on Li-loss to the gas phase

Due to the continuous flow of O_2/air over the powder bed during synthesis, it is unlikely that the full amount of H_2O that is released during the initial decomposition step in the calcination cycle will be available for recombination with Li_2O at higher temperatures during the cycle. However, it is not unreasonable to assume that due to diffusion limitations and non-ideal mixing within the powder bed, trace amounts of H_2O might be in the calcination atmosphere at high temperatures. To verify if this could significantly alter the calculated lithium volatilization of a "dry" system, the calculations from section 4.1 were repeated with identical inputs, but with the addition of a varying H_2O partial pressure in the system. The results of these calculations are shown in Fig. 5. The graph shows the mol% of lithium from the total lithium input of the system that ends up in the gas phase (mol Li_g per mol Li_{tot}) as a function of temperature for varying H_2O partial pressures. Comparing the graph of 1000 °C with the lithium loss at 1000 °C obtained in Fig. 2a, we can see that at a p_{H_2O} of just 10^{-6} atm (1 ppm H_2O in the gas phase), we find that lithium losses have increased by a factor of 100. This means that even under nominally dry, oxygen-enriched conditions, lithium volatility can be expected to be driven practically entirely by LiOH formation from residual water, with Li_2O_2 (and Li_2O) contributing negligibly to the total vapor pressure.

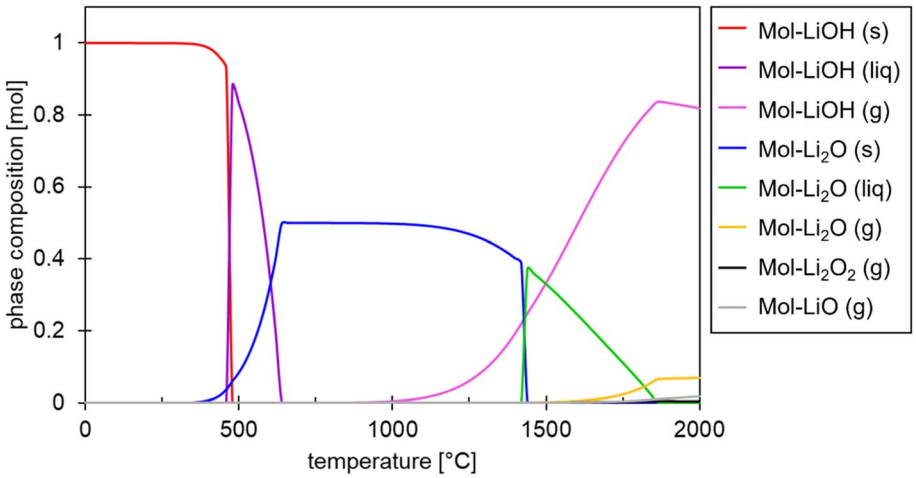

Fig. 3 Evolution of the phase composition of 1 mol LiOH under an O_2 atmosphere as function of temperature.

To put this into practical perspective, the results of a thermodynamical calculation, with adjusted inputs (Table S4 of the SI) to reflect the production of 1 kg NMC811 using 1 Nm^3 of O_2 containing varying levels of moisture ($p_{H_2O} = 0.001 - 1.0$ atm), is shown in Fig. 6. This calculation is handled as an open system, in which the total amount of gas ($O_2 + H_2O$) is added in discrete steps of 10l, and allowed to equilibrate with the solid phase. After every step the gas phase is removed, and the calculation proceeds with the adjusted solid phase in the next step. Hence, the calculation takes into consideration that fresh O_2 gas is continuously supplied to the solid interface and projects the predicted cumulative lithium loss after exposure to the total gas volume. The contour plot puts an important perspective on the relevance of lithium volatility during calcination. For processes executed between 800 °C and 900 °C, total lithium losses of just 10 mg are predicted for H_2O partial pressures < 0.01 atm per kg of synthesized NMC. While this 0.01% loss can become significant at high throughput from an economical perspective, it should not be expected to contribute to deterioration of performance. Hence, it should be not crucial to consider in the context of most lab scale investigations. While at temperatures above 900 °C and partial pressures above 0.01 atm the losses become increasingly significant, these circumstances should rarely occur during actual NMC synthesis.

The preceding sections focused on lithium volatility under pure O_2 atmospheres, as is standard for high Ni NMC synthesis. However, mid-nickel compositions (*e.g.* NMC532, NMC622) are commonly calcined in dry air, where CO_2 is present at approximately 420 ppm. To assess whether CO_2 introduces an additional lithium volatilization pathway, an equivalent equilibrium calculation was performed for the Li_2CO_3–O_2 system (Figure S1, SI). The results confirm that no volatile lithium-carbon-oxygen gas-phase species are formed at any temperature; the gas-phase lithium species remain identical to those in the dry Li–O system with equally negligible partial pressures. Hence, unlike H_2O which creates the highly volatile LiOH(g), CO_2 does not open a new volatilization channel for lithium. However, the calculations confirm that Li_2CO_3 remains thermodynamically stable as a condensed phase up to approximately 1150 °C under 1 atm O_2, existing as a solid below 750 °C and as a liquid between 750 °C and 1150 °C. In the presence of atmospheric CO_2, a fraction of the available lithium may therefore be stabilized as Li_2CO_3 rather than participating in the lithiation of the transition-metal precursor. This competing reaction effectively

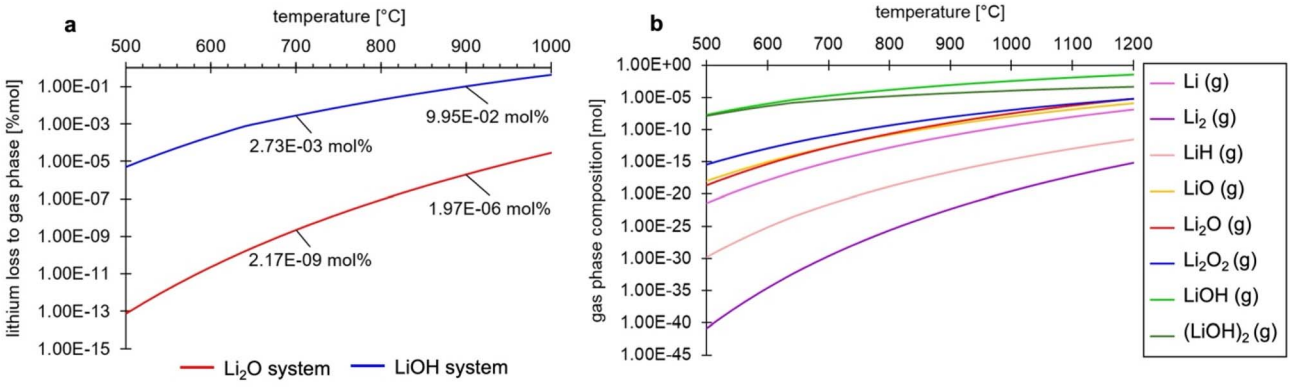

Fig. 4 Total lithium losses to the O_2–gas phase in the pure LiOH system (a). Vapor pressures of individual gaseous compounds that constitute the total lithium loss to the gas phase in the temperature interval relevant for NMC synthesis in the Li–O–H system (b).

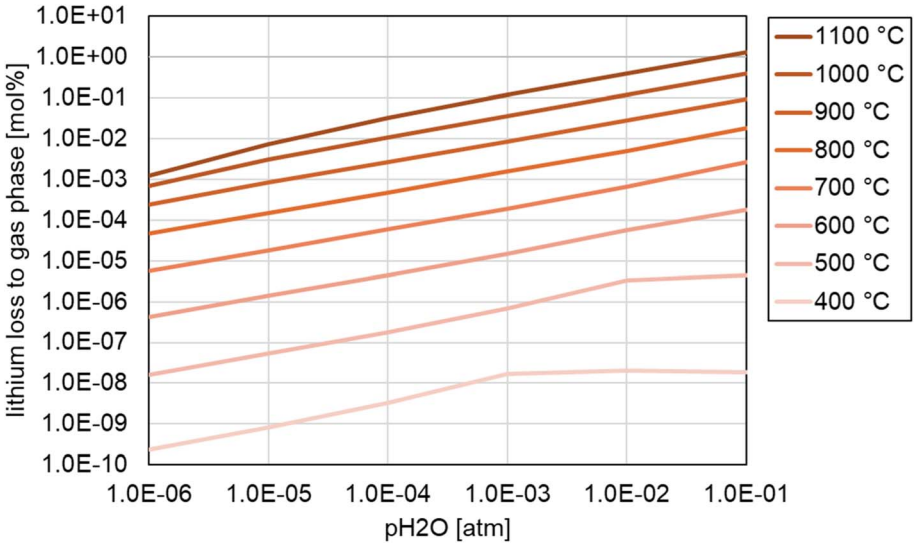

Fig. 5 Calculated lithium losses to the gas phase in a "wet" Li_2O system as a function of the water vapor partial pressure in the system.

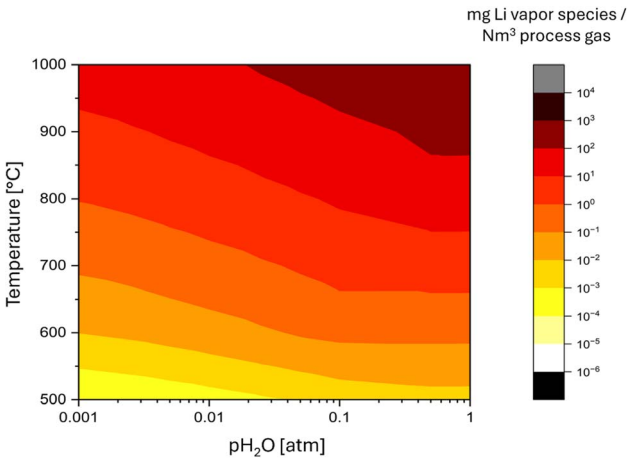

Fig. 6 Projected lithium losses on mass production under varying H_2O partial pressures in the gas supply.

sequesters lithium and delays its incorporation into the layered structure, consistent with the observations of McCalla *et al.*[13] who reported significantly higher lithium losses in air compared to pure O_2. While this mechanism does not constitute a volatilization loss (this lithium remains in the condensed phase) it can manifest as an apparent lithium deficiency in the final product if the Li_2CO_3 fails to fully decompose and react before the end of the calcination cycle. For processes conducted at 850–950 °C, as is typical for mid-nickel NMC compositions, this is particularly relevant given that Li_2CO_3 remains stable throughout this temperature range.[48,49]

4.4 Thermogravimetric analysis

To experimentally verify the predicted negligible volatility of lithium species at standard calcination temperatures, thermogravimetric analysis was performed on a stoichiometric (Li : $M = 1.00$) NMC($9\frac{11}{22}$) blend in an MgO crucible under O_2 flow. Fig. 7 shows the normalized mass and temperature as a function of time. Two distinct mass loss regions are identified during heating. Region I (~200–500 °C) corresponds to the thermal decomposition of LiOH and $TM(OH)_2$, releasing H_2O as the hydroxide precursors convert to their respective oxides. Region II (~800–900 °C) is attributed to the partial thermal decomposition of the nascent layered $LiTMO_2$ phase (following eqn. (3)), which becomes thermodynamically less stable at elevated temperatures, releasing a small amount of Li_2O and O_2 from the lattice. Upon reaching 900 °C, the mass remains constant throughout the 60 minute isothermal hold, with no detectable downward trend. For reference, the overall reaction $LiOH + TM(OH)_2 + 1/2O_2 \rightarrow LiTMO_2 + 3/2H_2O$ predicts a theoretical retained mass of 83.7% (approximately reached during ramp to 700 °C); a 1 mol% lithium loss by Li_2O evaporation would correspond to a ~0.15 percentage point monotonic decrease in normalized mass over the hold, which is approximately five times the ±0.03% baseline stability observed during the isothermal segment. No such trend is detected, directly confirming that lithium volatilization is negligible at typical NMC calcination temperatures, consistent with the thermodynamic predictions presented in Sections 4.1–4.3.

4.5 Calcination experiments

4.5.1 Effect of substrate contact area on lithium loss. The preceding thermodynamic analysis establishes that even under humid conditions ($p(H_2O) = 0.1$ atm) lithium volatilization cannot account for more than ~0.1 mol% loss at 900 °C, far below the 1–10 mol% observed experimentally. Evaporation is therefore insufficient to explain the lithium losses reported in the literature. The following calcination experiments identify the actual dominant mechanism: solid-state reaction between the cathode precursor and the substrate.

In previous work, we demonstrated that there exists at small length scales a clear correlation between lithium loss during calcination, and the substrate material used. The investigation outlined the relevant thermodynamic systems of Li_2O–SiO_2 and

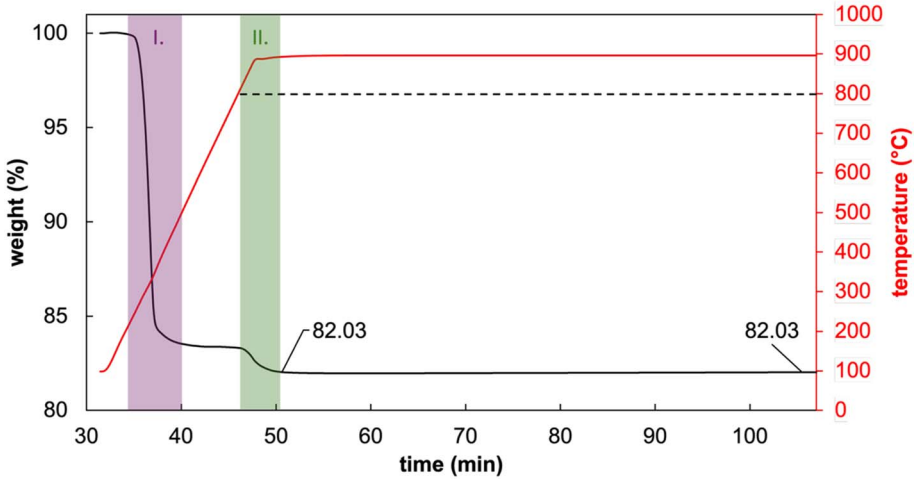

Fig. 7 TGA analysis of a stoichiometric NMC($9\frac{11}{22}$) blend (LiOH + $TM(OH)_2$) heated at 50 °C min^{-1} to 900 °C and held isothermally for 60 minutes in an MgO crucible under O_2 flow (100 mL min^{-1}). The normalized mass (black, left axis) and temperature (red, right axis) are shown as a function of time. Region I corresponds to the decomposition of LiOH and $TM(OH)_2$ with associated H_2O release. Region II corresponds to the partial thermal decomposition of the layered $LiTMO_2$ phase at elevated temperatures. The dashed line indicates the onset of $LiTMO_2$ decomposition. No mass loss is observed during the isothermal hold at 900 °C.

Li_2O–Al_2O_3, which illustrate that common oxide refractories have significant affinity for lithium compounds. It was verified experimentally that SiO_2 and Al_2O_3 substrates yield high lithium losses and effectively compete with the transition metal (TM) precursor for lithiation, by forming Li_4SiO_4 and $LiAlO_2$ layers at the substrate interface, respectively. Based on the thermodynamic investigation, and verified experimentally, it was shown that lithium loss can be significantly reduced by using substrates with lower affinity for lithium, such as MgO and Au. However, since SiO_2 and Al_2O_3 are still the industrial standards for lab scale investigations, we discuss here additional calcination experiments that aim to map the importance of lithium losses through parasitic side reactions, to compare their significance compared to theoretical evaporation losses.

Calcination experiments C1 and C2, as defined in section 3.3, essentially tested the same parameter: the influence of the A/m ratio on total lithium losses during a single calcination cycle. ICP Results from C1 are shown in Table 2, where C1 – A is the reference calcination, and C1 – B is the calcination with increased Al_2O_3 contact surface area. This data shows that increasing this ratio for the same blend mass, by dispersing Al_2O_3 fragments in the powder blend, thereby artificially increasing the A/m ratio, leads to a considerable increase in lithium losses. From the results of C2, a straightforward quantification could be obtained, as in this experiment the A/m ratio could easily be calculated for each crucible, by measuring the powder height in each crucible.

Fig. 8 presents the results of ICP measurements quantifying lithium loss in NMC cathode material after calcination in three different crucible materials: silica fiber, silica quartz, and alumina. The *x*-axis shows the contact surface area between the NMC powder and the crucible (A/m, in mm^2 g^{-1}), while the *y*-axis indicates the percentage decrease in the Li : M ratio, representing lithium loss.

A clear linear relationship is observed for all three crucible types: as the contact surface area increases, lithium loss also increases. This trend is highly consistent, as indicated by the high R^2 values for each fit (silica fiber: 0.999, silica quartz: 0.9943, alumina: 0.9965). Among the crucibles, silica fiber shows the steepest slope, indicating the highest sensitivity of lithium loss to increased contact area, followed by silica quartz and finally alumina.

This linear dependence strongly suggests that lithium loss during calcination is dominated by interfacial reactions between the NMC powder and the crucible material. As the available contact area increases, more lithium is in contact with the interface and will react with the crucible, forming stable lithium-containing compounds (such as $LiAlO_2$ with alumina or lithium silicates with silica-based crucibles). The differences in

Table 2 ICP-OES compositional analysis of samples from calcination experiment C1. Sample C1–A was calcined in an Al_2O_3 crucible under standard conditions, while sample C1–B was calcined under identical time and temperature conditions but with an increased Al_2O_3 contact surface area

	Li (wt%)	Ni (wt%)	Mn (wt%)	Co (wt%)	Li : M	Li loss (mol%)
Blend	6.75	44.5	5.31	5.63	1.04	—
C1 – A	7.06	47.53	5.63	6.00	1.00	3.7%
C1 – B	6.93	47.8	5.68	6.04	0.98	5.6%

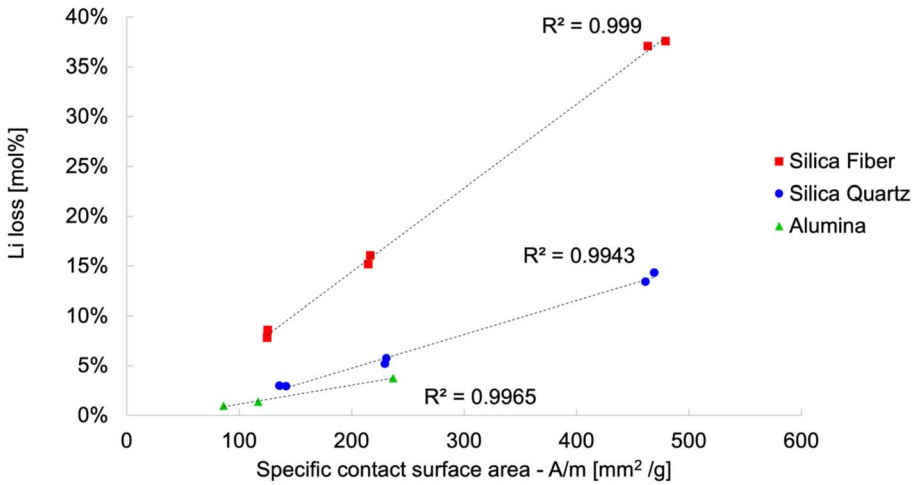

Fig. 8 Li loss during calcination as a function of specific contact surface area (A/m) for NMC calcined on three different substrate materials: silica fiber, silica quartz, and alumina. Linear fits are shown for each substrate type, with corresponding R^2 values indicated. The specific contact surface area is defined as the crucible contact area divided by the NMC blend mass.

slope between the crucible types reflect their varying reactivity with lithium.

4.5.2 Substrate saturation by repeated calcination. The results of calcination experiment C5, in which crucibles were reused for consecutive calcination cycles without cleaning, are shown in Fig. 9. For Al_2O_3 crucibles, lithium loss decreased progressively from 5.3 ± 0.1% in a fresh crucible to 3.5 ± 0.2% after one prior use and 2.8 ± 0.1% after two prior uses (averages ± range across two repeats). This trend was independently corroborated by the Al content detected in the calcined NMC product, which decreased from 0.018 wt% (1st use) to 0.0078 wt% (2nd use) and 0.0053 wt% (3rd use), confirming that the extent of the Li_2O–Al_2O_3 reaction diminishes as the crucible interface becomes progressively passivated by a $LiAlO_2$ layer. MgO crucibles exhibited a qualitatively similar but less pronounced effect: lithium loss decreased from 1.9 ± 0.1% (1st use) to 1.2 ± 0.2% (2nd use), after which no further significant decrease was observed (3rd use: 1.4 ± 0.2%). The more rapid saturation of MgO is consistent with its lower thermodynamic affinity for lithium, as discussed in our previous work.[40] Importantly, the clear dependence of lithium loss on crucible usage history cannot be explained by an evaporation mechanism, as gas-phase volatilization is independent of the chemical state of the crucible surface. The observed saturation behavior is, however, fully consistent with a substrate-interaction mechanism in which the available reactive surface area is gradually consumed by the formation of stable lithium-containing phases at the crucible interface. These results also carry practical implications: in laboratory settings where crucibles are routinely reused, the lithium loss measured in successive experiments will systematically underestimate the losses that would occur in a fresh crucible, potentially introducing an unrecognized source of variability between studies.

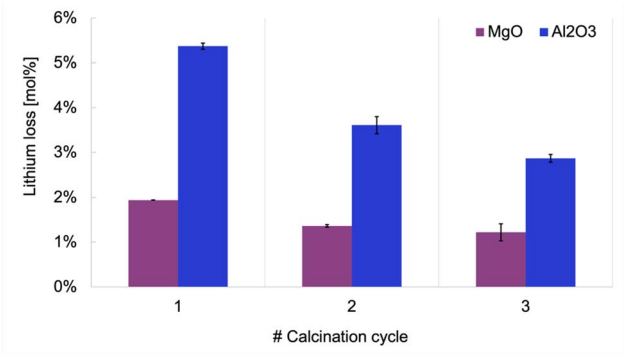

Fig. 9 Lithium loss (mol%) as a function of repeated calcination cycles for NMC811 blends calcined in MgO and Al_2O_3 crucibles under identical conditions. Error bars represent the standard deviation of replicate experiments. The decreasing lithium loss with successive cycles is consistent with progressive passivation of the crucible surface through the formation of stable lithium-containing phases ($LiAlO_2$ for Al_2O_3, limited solid solution for MgO), which reduce the availability of reactive surface sites for further lithium uptake.

4.5.3 Lithium gradient through the sintered body. The Li : M gradient as measured by ICP in separate layers of the calcined sample from experiment C3 through a sintered sample with thickness 1.2 cm is shown in Fig. 10, where 0 cm coincides with the atmosphere contact surface and 1.2 cm with the crucible contact surface. Data points were obtained by separately sampling individual layers of the sintered specimen. The Li : M has a local maximum 0.2 cm below the powder surface and shows a steep negative gradient towards the crucible contact surface. This indicates lithium is lost by diffusion in two directions: The majority of lithium diffuses towards the crucible, where it is lost to crucible interaction. A small amount diffuses towards the powder surface where it presumably moves to the gas phase. This illustrates that in the performed experiment, the contribution of crucible interactions to the Li-losses largely outweighs the contribution of possible evaporation phenomena. Since the experiment was performed in the non-porous and commonly used alumina crucible, it shows once

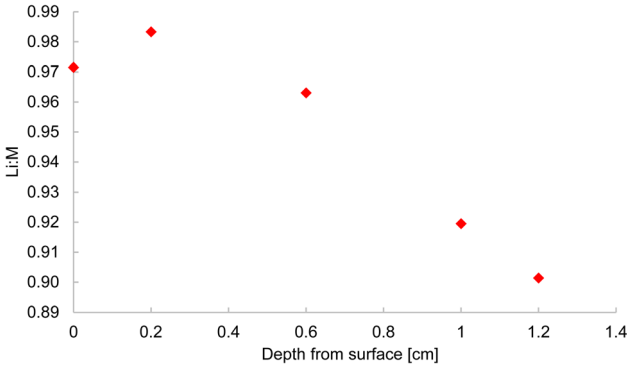

Fig. 10 Li : M ratio as function of depth from the sample surface.

more that the measured decrease in the overall Li/M ratio in lab-scale experiments should be attributed mostly to crucible interaction, rather than lithium evaporation from solid solution.

4.5.4 Effect of moisture on lithium loss and electrochemical performance. Fig. 11 shows coin cell results from the final calcination experiment C4, illustrating the effect of H_2O vapor pressure on high temperature lithium losses of NMC blend in selected crucibles, by saturating the furnace atmosphere with H_2O. After the experiments, samples were taken for ICP-OES analyses and electrochemical testing. The cycling protocol used for the electrochemical tests is outlined in 50 and serves as a time efficient evaluation of performance under varying conditions. The first part (cycle 1–6) represents the evaluation of rate performance at discharge rates of 0.1C, 0.2C, 0.5C, 1C, 2C and 3C in the 4.3–3.0 V/Li metal window range. The second part (cycle 7–35) serves as evaluation of the cycle life at 1C. The charge cut-off voltage is set at 4.5 V/Li metal. The discharge capacity is measured at 0.1C at cycles 7 and 34 and 1C at cycles 8 and 35 to evaluate capacity fading in both conditions after 24 cycles at constant C-rate. Two coin cells were measured for each obtained cathode material. Fig. 11a represents the performance of reference materials produced under standard (Dry) conditions in different crucibles. As mentioned before, our earlier work outlines a clear substrate dependency of both lithium loss and electrochemical performance.[40] While the cycle stability of the reference cathodes produced in Al_2O_3 and SiO_2 quartz (SiO_2 (Q)) are comparable, there is a significant difference in overall discharge capacity, with the cathodes from Au and MgO outperforming by 4%–6% over the entire cycling protocol. The magnitude of this capacity difference correlates well with the difference in lithium loss measured from ICP listed in Table 3: MgO – 1.9%; Au – 1.9%; SiO (Q) – 7.0%; Al_2O_3 – 6.0%. On the other hand, the cathode material produced in SiO_2 (F) shows both an extremely low initial capacity, as well as a notably lower cycle stability, losing nearly its complete capacity over just 35 cycles. For a more detailed analysis, the authors refer to.[40] Noteworthy in the context of the current work, is the comparison to Fig. 11b, which represents the cyclic performance of cathode materials produced in the same crucibles, but under wet conditions. Table 3 captures

Table 3 ICP results from Dry and Wet calcination

Sample	Li loss (mol%)
SiO (F) – dry	29.6
SiO (F) – wet	50.9
SiO (Q) – dry	7.0
SiO (Q) – wet	14.1
Al_2O_3 – dry	6.0
Al_2O_3 – wet	11.8
Au – dry	1.9
Au – wet	7.4
MgO – dry	1.9
MgO – wet	6.8

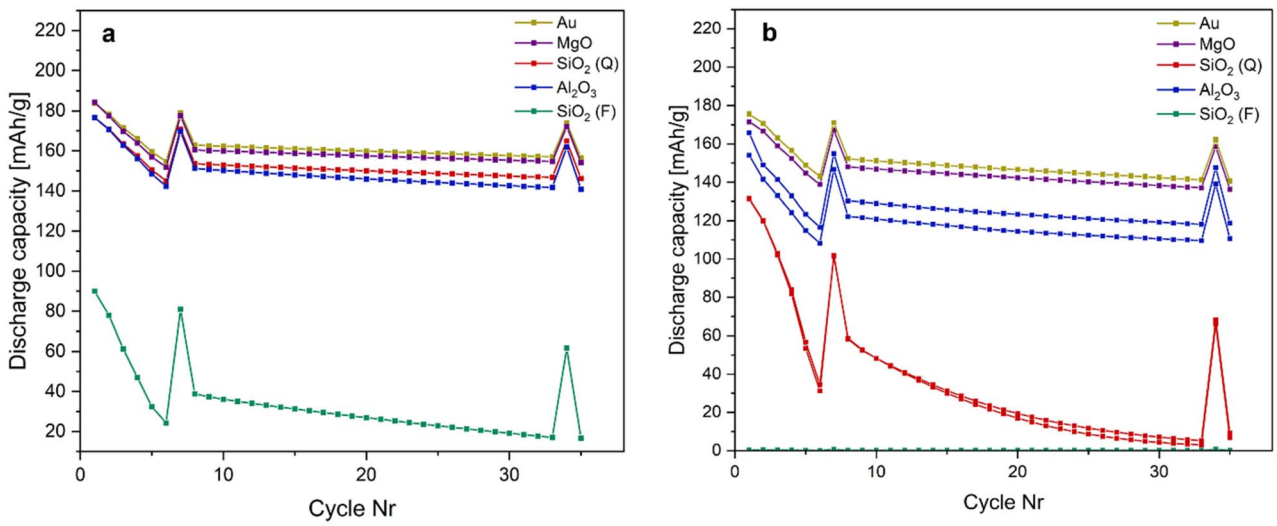

Fig. 11 Coin cell data of calcination experiment C4. Specific discharge capacity over the full cycling protocol of cathodes produced by (dry) reference sintering in different crucibles (a). Specific discharge capacity over the full cycling protocol of cathodes produced by (wet) sintering under saturated H_2O atmosphere in different crucibles (b).

unambiguously the increase in total lithium losses by introduction of H_2O into the synthesis system. The increase in volatility is different for each crucible: While both MgO and Au increase lithium loss under wet conditions by a factor of approximately 3.5, both SiO_2 (Q) and Al_2O_3 show an increase with factor ~2, and SiO_2 (F) with factor ~1.7. Most likely this is because increasing the H_2O partial pressure not only increases the vapor pressure of lithium species but can also lead to hydration reactions of the crucible materials, which might affect both the mechanism and scale of lithium losses through solid state substrate interaction. However, the impact on performance is clear. Cathode materials produced in Al_2O_3, SiO_2 quartz, MgO and Au show a notable decrease in both initial discharge capacity and cycle stability when compared with their reference, while the cathode material produced in SiO_2 (F) shows no signs of electrochemical activity. Since the lithium loss of this last sample exceeds 50%, this is likely because of the absence of a sufficient fraction electrochemically active layered ($R\bar{3}m$) layered structure due to off-stoichiometry. The electrochemical data provide direct functional evidence that substrate-induced lithium loss, and not evaporation, governs cathode performance under standard synthesis conditions. The 4–6% capacity gap between inert (MgO, Au) and reactive (Al_2O_3, SiO_2) substrates is fully consistent with the ICP-measured lithium deficiencies and cannot be explained by a gas-phase volatilization mechanism, which would affect all substrates equally. Under humid conditions, the additional LiOH(g)-mediated volatilization further degrades performance across all substrates, confirming moisture as a secondary but significant loss pathway. Together, these results establish a clear hierarchy: substrate reactivity is the primary source of lithium loss under dry calcination, while moisture-assisted volatilization becomes relevant only when H_2O is present in the furnace atmosphere.

5 Conclusion

Contrary to the prevailing explanation in the literature, lithium loss during NMC cathode synthesis is not caused by Li_2O evaporation. Thermodynamic analysis demonstrates that gaseous lithium species remain negligible ($<3 \times 10^{-5}$ mol%) throughout the entire calcination temperature range under dry conditions, about 5 orders of magnitude below reported experimental losses. However, thermodynamic calculations reveal that even trace amounts of water vapor, substantially increase lithium volatility through LiOH(g) formation, making moisture control a critical factor for maintaining stoichiometric precision. Nevertheless, the total lithium loss predicted under even relatively humid conditions ($p(H_2O) = 0.1$ atm) remains below 0.1%, far less than the 1–10 mol% typically reported in experimental studies. Complementary calcination experiments clarify this discrepancy, demonstrating that the predominant source of lithium loss is not volatilization but solid-state interfacial reactions between the cathode precursor and the crucible material. Lithium readily reacts with common oxidic refractories such as SiO_2 and Al_2O_3, forming stable lithium silicates and aluminates, with losses scaling linearly with the crucible–powder contact area. In contrast, MgO and Au substrates exhibit minimal reactivity and effectively suppress lithium depletion. Depth-profile and electrochemical data further confirm that interfacial diffusion toward reactive substrates is the dominant lithium loss pathway, while evaporation contributes only marginally under standard conditions. Under wet calcination, increased H_2O partial pressure amplifies both lithium volatility and crucible reactivity, resulting in pronounced lithium deficiency and degraded electrochemical performance. Overall, these findings show that lithium volatility is thermodynamically negligible in dry air. Parasitic reactions at crucible interfaces and moisture-assisted volatilization represent the primary mechanisms of lithium loss during cathode synthesis. This underlines the need for optimized substrate selection and strict atmosphere control in both laboratory and industrial processes.

Conflicts of interest

The authors declare that they have no known competing financial interests or personal relationships that could have appeared to influence the work reported in this paper.

Data availability

The data that support the findings of this study are openly available in the Open Science Framework (OSF) repository at https://osf.io/krczh, reference ID: KRCZH.

Supplementary information (SI) is available. See DOI: https://doi.org/10.1039/d6ta02981g.

Acknowledgements

S. Coessens holds a grant [HBC.2022.0157] which is supported by VLAIO, the Flanders Innovation & Entrepreneurship Agency, in co-operation with Umicore. I. Bellemans holds a grant from the Research Foundation Flanders (1239024N).

References

1 N. Nitta, F. Wu, J. T. Lee and G. Yushin, Li-ion battery materials: present and future, *Mater. Today*, 2015, **18**(5), 252–264, DOI: 10.1016/j.mattod.2014.10.040.

2 F. Schipper, E. M. Erickson, C. Erk, J. Y. Shin, F. F. Chesneau and D. Aurbach, Recent Advances and Remaining Challenges for Lithium Ion Battery Cathodes: I. Nickel-Rich, $LiNi_xCo_yMn_zO_2$, *J. Electrochem. Soc.*, 2017, **164**(1), A6220–A6228, DOI: 10.1149/2.0351701jes.

3 C. M. Julien and A. Mauger, NCA, NCM811, and the Route to Ni-Richer Lithium-Ion Batteries, *Energies*, 2020, **13**(23), 6363, DOI: 10.3390/en13236363.

4 M. Malik, K. H. Chan and G. Azimi, Review on the synthesis of $LiNi_xMn_yCo_{1-x-y}O_2$ (NMC) cathodes for lithium-ion batteries, *Mater. Today Energy*, 2022, **28**, 101066, DOI: 10.1016/j.mtener.2022.101066.

5 J. Zhu, T. Vo, D. Li, *et al.*, Crystal Growth of $LiNi_{1/3}Co_{1/3}Mn_{1/3}O_2$ as a Cathode Material for High-

Performance Lithium Ion Batteries, *Cryst. Growth Des.*, 2012, **12**(3), 1118–1123, DOI: 10.1021/cg200565n.

6 K. Fröhlich, E. Legotin, F. Bärhold and A. Trifonova, New large-scale production route for synthesis of lithium nickel manganese cobalt oxide, *J. Solid State Electrochem.*, 2017, **21**(12), 3403–3410, DOI: 10.1007/s10008-017-3644-x.

7 D. Wang, R. Kou, Y. Ren, *et al.*, Synthetic Control of Kinetic Reaction Pathway and Cationic Ordering in High-Ni Layered Oxide Cathodes, *Adv. Mater.*, 2017, **29**(39), 1606715, DOI: 10.1002/adma.201606715.

8 M. Bianchini, F. Fauth, P. Hartmann, T. Brezesinski and J. Janek, An *in situ* structural study on the synthesis and decomposition of $LiNiO_2$, *J. Mater. Chem. A*, 2020, **8**(4), 1808–1820, DOI: 10.1039/C9TA12073D.

9 M. Gao, Y. He, K. Yan, *et al.*, Synthesizing kinetics and characteristics of high-capacity $Li_{1.16}(Ni_{0.25}Mn_{0.75})_{0.84}O_2$ cathode materials for lithium-ion batteries, *Ionics*, 2021, **27**(9), 3729–3737, DOI: 10.1007/s11581-021-04068-z.

10 S. Jo, J. Han, S. Seo, *et al.*, Solid-State Reaction Heterogeneity During Calcination of Lithium-Ion Battery Cathode, *Adv. Mater.*, 2023, **35**(10), 2207076, DOI: 10.1002/adma.202207076.

11 T. Sata, High-Temperature Vaporization of Li_2O Component from Solid Solution $Li_xNi_{1-x}O_2$ in Air, *Ceram. Int.*, 1996, **24**, 53–59.

12 E. Antolini, On Li_2O evaporation from $Li_xNi_{1-x}O$ solid solution, *Ceram. Int.*, 1999, **25**(7), 677–679, DOI: 10.1016/S0272-8842(98)00073-X.

13 E. McCalla, G. H. Carey and J. R. Dahn, Lithium loss mechanisms during synthesis of layered $Li_xNi_{2-x}O_2$ for lithium ion batteries, *Solid State Ionics*, 2012, **219**, 11–19, DOI: 10.1016/j.ssi.2012.05.007.

14 J. Li, G. Liang, W. Zheng, *et al.*, Addressing cation mixing in layered structured cathodes for lithium-ion batteries: A critical review, *Nano Mater. Sci.*, 2023, **5**(4), 404–420, DOI: 10.1016/j.nanoms.2022.09.001.

15 T. E. Ashton, P. J. Baker, C. Sotelo-Vazquez, *et al.*, Stoichiometrically driven disorder and local diffusion in NMC cathodes, *J. Mater. Chem. A*, 2021, **9**(16), 10477–10486, DOI: 10.1039/D1TA01639C.

16 F. Guo, Y. Xie and Y. Zhang, Tuning Li-excess to optimize Ni/Li exchange and improve stability of structure in $LiNi_{0.8}Co_{0.1}Mn_{0.1}O_2$ cathode material for lithium-ion batteries, *Nano Res.*, 2022, **15**(10), 8962–8971, DOI: 10.1007/s12274-022-4532-y.

17 F. Wu, J. Tian, Y. Su, *et al.*, Effect of Ni^{2+} Content on Lithium/Nickel Disorder for Ni-Rich Cathode Materials, *ACS Appl. Mater. Interfaces*, 2015, **7**(14), 7702–7708, DOI: 10.1021/acsami.5b00645.

18 B. T. Truong, Y. S. Wu, T. F. Hung, *et al.*, The effect of lithium-excess on Ni-rich $LiNi_{0.6}Co_{0.2}Mn_{0.2}O_2$ cathode materials prepared by a Taylor flow reactor, *Electrochim. Acta*, 2021, **391**, 138982, DOI: 10.1016/j.electacta.2021.138982.

19 Y. Kim, H. Park, J. H. Warner and A. Manthiram, Unraveling the Intricacies of Residual Lithium in High-Ni Cathodes for Lithium-Ion Batteries, *ACS Energy Lett.*, 2021, **6**(3), 941–948, DOI: 10.1021/acsenergylett.1c00086.

20 Y. Iida, Evaporation of Lithium Oxide from Solid Solution of Lithium Oxide in Nickel Oxide, *J. Am. Ceram. Soc.*, 1960, **43**(3), 171–172, DOI: 10.1111/j.1151-2916.1960.tb14336.x.

21 Y. Ikeda, A Mass Spectrometric Study of Vaporization of Li_2O with Some Refractory Metal Cells, *J. Mass Spectrom. Soc. Jpn.*, 1979, **27**(4), 263–273.

22 B. Konar, M. A. Van Ende and I. H. Jung, Critical evaluation and thermodynamic optimization of the Li-O, and Li_2O-SiO_2 systems, *J. Eur. Ceram. Soc.*, 2017, **37**(5), 2189–2207, DOI: 10.1016/j.jeurceramsoc.2016.12.041.

23 E. Antolini, Sintering of $Li_xNi_{1-x}O$ solid solutions at 1200°C, *J. Mater. Sci.*, 1992, **27**, 3335–3340.

24 E. Antolini, Kinetics of Li_2O evaporation from lithium-rich $Li_xNi_{1-x}O$ solid solutions at 870 °C, *J. Mater. Sci. Lett.*, 1994, **13**, 1599–1601.

25 E. Antolini, $Li_xNi_{1-x}O$ ($0<x\leq0.3$) solid solutions: formation, structure and transport properties, *Mater. Chem. Phys.*, 2003, **82**(3), 937–948, DOI: 10.1016/j.matchemphys.2003.08.006.

26 E. Antolini, Formation of $Li_xNi_{1-x}O$ solid solution from Ni/Li_2CO_3 mixtures, *Mater. Lett.*, 1993, **16**(5), 286–290, DOI: 10.1016/0167-577X(93)90193-2.

27 D. Wang, C. Xin, M. Zhang, *et al.*, Intrinsic Role of Cationic Substitution in Tuning Li/Ni Mixing in High-Ni Layered Oxides, *Chem. Mater.*, 2019, **31**(8), 2731–2740, DOI: 10.1021/acs.chemmater.8b04673.

28 F. Klein, C. Pfeifer, P. Scheitenberger, *et al.*, In-depth structural characterization of the influence of Li^+ excess on spherical, Co-free layered $LiMn_{0.5}$ $Ni_{0.5}$ O_2 cathode material using correlative Raman–SEM microscopy, *J. Mater. Chem. A*, 2023, **11**(10), 5135–5147, DOI: 10.1039/D2TA05957F.

29 B. Wu, R. Yi, Y. Xu, *et al.*, Unusual Li_2O sublimation promotes single-crystal growth and sintering, *Nat. Energy*, 2025, **10**(5), 605–615, DOI: 10.1038/s41560-025-01738-4.

30 K. Estala-Rodriguez, S. Cordova and E. Shafirovich, Oxidation and combustion of stabilized lithium metal powder (SLMP), *Proc. Combust. Inst.*, 2023, **39**(3), 3583–3592, DOI: 10.1016/j.proci.2022.07.051.

31 R. A. Nefedov, Y. A. Ferapontov and N. P. Kozlova, Problem of the lithium peroxide thermal stability, *IOP Conf. Ser. Mater. Sci. Eng.*, 2016, **112**, 012027, DOI: 10.1088/1757-899X/112/1/012027.

32 K. P. C. Yao, D. G. Kwabi, R. A. Quinlan, *et al.*, Thermal Stability of Li_2 O_2 and Li_2 O for Li-Air Batteries: In Situ XRD and XPS Studies, *J. Electrochem. Soc.*, 2013, **160**(6), A824–A831, DOI: 10.1149/2.069306jes.

33 H. Beyer, S. Meini, N. Tsiouvaras, M. Piana and H. A. Gasteiger, Thermal and electrochemical decomposition of lithium peroxide in non-catalyzed carbon cathodes for Li–air batteries, *Phys. Chem. Chem. Phys.*, 2013, **15**(26), 11025, DOI: 10.1039/c3cp51056e.

34 A. E. V. Arkel, U. Spitsbergen and R. D. Heyding, Note on the volatility of Lithium Oxide, *Can. J. Chem.*, 1955, **33**(2), 446–447.

35 K. Watari, H. J. Hwang, M. Toriyama and S. Kanzaki, Effective Sintering Aids for Low-temperature Sintering of AlN Ceramics, *J. Mater. Res.*, 1999, **14**, 14, DOI: 10.1557/JMR.1999.0191.

36 T. Hoshino, Pebble fabrication of super advanced tritium breeders using a solid solution of $Li_{2+x}TiO_{3+y}$ with Li_2ZrO_3, *Nucl. Mater. Energy*, 2016, **9**, 221–226.

37 W. Lan, D. Lu, R. Zhao and H. Chen, Investigation of Al_2O_3 Crucible Contamination induced by extra Li_2CO_3 during $Li_7La_3Zr_2O_{12}$ Solid Electrolyte Sintering process, *Int. J. Electrochem. Sci.*, 2019, **14**(10), 9695–9703, DOI: 10.20964/2019.10.22.

38 C. W. Bale, E. Bélisle, P. Chartrand, *et al.*, FactSage thermochemical software and databases — recent developments, *Calphad*, 2009, **33**(2), 295–311, DOI: 10.1016/j.calphad.2008.09.009.

39 C. W. Bale, E. Bélisle, P. Chartrand, *et al.*, FactSage thermochemical software and databases, 2010–2016, *Calphad*, 2016, **54**, 35–53, DOI: 10.1016/j.calphad.2016.05.002.

40 S. Coessens, B. Bahramian, I. Bellemans, T. Crivits, C. Detavernier and K. Verbeken, On the sensitivity of ternary lithium-ion cathode materials to substrate-induced lithium loss during calcination, *J. Eur. Ceram. Soc.*, 2026, **46**(7), 118124, DOI: 10.1016/j.jeurceramsoc.2025.118124.

41 T. L. Kinnibrugh, P. Barai, J. C. Garcia, *et al.*, Thermodynamic and Kinetic Mechanisms Governing the Synthesis of Nickel-Poor Cathodes, *Chem. Mater.*, 2025, **37**(16), 6256–6270, DOI: 10.1021/acs.chemmater.5c01173.

42 N. T. T. Tran, C. a. Lin and S. k. Lin, Insights into the Structural and Thermodynamic Instability of Ni-Rich NMC Cathode, *ACS Sustainable Chem. Eng.*, 2023, **11**(18), 6978–6987, DOI: 10.1021/acssuschemeng.2c07428.

43 M. W. Chase, NIST-JANAF Thermochemical Tables, in *NIST-JANAF Thermochemical Tables*, Journal of Physical and Chemical Reference Data, Monograph, American Institute of Physics, 1998, 4th edn, pp. 1–1951. https://janaf.nist.gov/janaf4pdf.html.

44 P. Kurzhals, F. Riewald, M. Bianchini, *et al.*, Deeper Understanding of the Lithiation Reaction during the Synthesis of $LiNiO_2$ Towards an Increased Production Throughput, *J. Electrochem. Soc.*, 2022, **169**(5), 050526, DOI: 10.1149/1945-7111/ac6c0b.

45 L. N. Dinh, D. M. Grant, M. A. Schildbach, *et al.*, Kinetic measurement and prediction of the hydrogen outgassing from the polycrystalline LiH/Li2O/LiOH system, *J. Nucl. Mater.*, 2005, **347**(1–2), 31–43, DOI: 10.1016/j.jnucmat.2005.06.025.

46 J. Sicklinger, M. Metzger, H. Beyer, D. Pritzl and H. A. Gasteiger, Ambient Storage Derived Surface Contamination of NCM811 and NCM111: Performance Implications and Mitigation Strategies, *J. Electrochem. Soc.*, 2019, **166**(12), A2322–A2335, DOI: 10.1149/2.0011912jes.

47 L. V. Gurvich, G. A. Bergman, L. N. Gorokhov, V. S. Iorish, V. Ya Leonidov and V. S. Yungman, Thermodynamic Properties of Alkali Metal Hydroxides. Part 1. Lithium and Sodium Hydroxides, *J. Phys. Chem. Ref. Data*, 1996, **25**(4), 1211–1276, DOI: 10.1063/1.555982.

48 R. D. Endah, T. Paramitha, A. Jumari, *et al.*, Tuning of Nickel Content in High-Layered $LiNi_xMn_yCo_zO_2$ (NMC) from Spent Catalyst, *Evergreen*, 2024, **11**(3), 2265–2272, DOI: 10.5109/7236869.

49 I. Ben-Barak and M. N. Obrovac, All-Dry Synthesis of NMC from $[Ni,Mn,Co]_3$ O_4 Spinel Precursors, *J. Electrochem. Soc.*, 2024, **171**(4), 040535, DOI: 10.1149/1945-7111/ad3aa9.

50 J. Kim, J. Paulsen. Ni based Cathode Material for Rechargeable Lithium-Ion Batteries. *US Pat.*0123347, 2019.

